# Explicit solid dynamics in OpenFOAM

**Jibran Haider** [a], Chun Hean Lee [a], Antonio J. Gil [a], Javier Bonet [b] and Antonio Huerta [c]

m.j.haider@swansea.ac.uk

[a] Zienkiewicz Centre for Computational Engineering, College of Engineering, Swansea University, Bay Campus, SA1 8EN, United Kingdom

[b] University of Greenwich, London, SE10 9LS, United Kingdom

[c] Laboratory of Computational Methods and Numerical Analysis (LaCàN), Universitat Politècnica de Catalunya, UPC BarcelonaTech, 08034, Barcelona, Spain

**Abstract:**

An industry-driven computational framework for the numerical simulation of large strain explicit solid dynamics is presented. This work focuses on the spatial discretisation of a system of first order hyperbolic conservation laws using the cell centred Finite Volume Method [1, 2, 3]. The proposed methodology has been implemented as a parallelised explicit solid dynamics tool-kit within the CFD-based open-source platform OpenFOAM. Crucially, the proposed framework bridges the gap between Computational Fluid Dynamics and large strain solid dynamics. A wide spectrum of challenging numerical examples are examined in order to assess the robustness and parallel performance of the proposed solver.

## 1 Introduction

Current commercial codes (e.g. ESI-VPS, PAM-CRASH, LS-DYNA, ANSYS AUTODYN, ABAQUS, Altair HyperCrash) used in industry for the simulation of large-scale solid mechanics problems are typically based on the use of traditional second order displacement based Finite Element formulations. However, it is well-known that these formulations present a number of shortcomings, namely (1) reduced accuracy for strains and stresses in comparison with displacements; (2) high frequency noise in the vicinity of shocks; and (3) numerical instabilities associated with shear (or bending) locking, volumetric locking and pressure checker-boarding.

Over the past few decades, various attempts have been reported at aiming to solve solid mechanics problems using the displacement-based Finite Volume Method [4, 5, 6]. However, most of the proposed methodologies have been restricted to the case of small strain linear elasticity, with very limited effort directed towards dealing with large strain nearly incompressible materials.

To address these shortcomings identified above, a novel mixed-based methodology tailor-made for emerging (industrial) solid mechanics problems has been recently proposed [1, 2, 3, 7, 8, 9, 10, 11, 12]. The mixed-based approach is written in the form of a system of first order hyperbolic conservation laws. The primary variables of interest are linear momentum and deformation gradient (also known as fibre map). Essentially,

the formulation has been proven to be very efficient in simulating sophisticated dynamical behaviour of a solid [2].

## 2 Governing equations

Consider the three dimensional deformation of an elastic body moving from its initial configuration occupying a volume $\Omega_0$, of boundary $\partial\Omega_0$, to a current configuration at time $t$ occupying a volume $\Omega$, of boundary $\partial\Omega$. The motion is defined through a deformation mapping $\boldsymbol{x} = \boldsymbol{\phi}(\boldsymbol{X}, t)$ which satisfies the following set of mixed-based Total Lagrangian conservation laws [1, 7, 8, 9, 10, 11, 12]

$$\frac{\partial \boldsymbol{p}}{\partial t} = \mathrm{DIV}\boldsymbol{P} + \boldsymbol{f}_0; \tag{1a}$$

$$\frac{\partial \boldsymbol{F}}{\partial t} = \mathrm{DIV}\left(\frac{1}{\rho_0}\boldsymbol{p} \otimes \boldsymbol{I}\right). \tag{1b}$$

Here, $\boldsymbol{p}$ represents the linear momentum per unit of undeformed volume, $\rho_0$ is the material density, $\boldsymbol{F}$ is the deformation gradient (or fibre map), $\boldsymbol{P}$ is the first Piola-Kirchhoff stress tensor, $\boldsymbol{f}_0$ is a material body force term, $\boldsymbol{I}$ is the second-order identity tensor and DIV represents the material divergence operator [10]. The above system (1a-1b) can alternatively be written in a concise manner as

$$\frac{\partial \boldsymbol{\mathcal{U}}}{\partial t} = \frac{\partial \boldsymbol{\mathcal{F}}_I}{\partial X_I} + \boldsymbol{\mathcal{S}}; \qquad \forall\, I = 1, 2, 3, \tag{2}$$

where $\boldsymbol{\mathcal{U}}$ is the vector of conserved variables and $\boldsymbol{\mathcal{F}}_I$ is the flux vector in the $I$-th material direction and $\boldsymbol{\mathcal{S}}$ is the material source term. Their respective components are

$$\boldsymbol{\mathcal{U}} = \begin{bmatrix} \boldsymbol{p} \\ \boldsymbol{F} \end{bmatrix}, \qquad \boldsymbol{\mathcal{F}}_{\boldsymbol{N}} = \boldsymbol{\mathcal{F}}_I N_I = \begin{bmatrix} \boldsymbol{P}\boldsymbol{N} \\ \frac{1}{\rho_0}\boldsymbol{p} \otimes \boldsymbol{N} \end{bmatrix}, \qquad \boldsymbol{\mathcal{S}} = \begin{bmatrix} \boldsymbol{f}_0 \\ \boldsymbol{0} \end{bmatrix}; \tag{3}$$

with $\boldsymbol{N}$ being the material unit outward surface normal vector. For closure of system (2), it is necessary to introduce an appropriate constitutive model to relate $\boldsymbol{P}$ with $\boldsymbol{F}$, obeying the principle of objectivity and thermodynamic consistency. Finally, for the complete definition of the Initial Boundary Value Problem (IBVP), initial and boundary (essential and natural) conditions must also be specified.

## 3 Numerical methodology

From the spatial discretisation viewpoint, the above system (2) is discretised using the standard cell centred finite volume algorithm as shown in Figure 1. The application of the Gauss divergence theorem on the integral form of (2) leads to its spatial approximation for an arbitrary cell $e$,

$$\frac{d\boldsymbol{\mathcal{U}}_e}{dt} = \frac{1}{\Omega_0^e}\int_{\Omega_0^e} \frac{\partial \boldsymbol{\mathcal{F}}_I}{\partial X_I}\, d\Omega_0 = \frac{1}{\Omega_0^e}\int_{\partial\Omega_0^e} \boldsymbol{\mathcal{F}}_{\boldsymbol{N}}\, dA \approx \frac{1}{\Omega_0^e}\sum_{f\in\Lambda_e^f} \boldsymbol{\mathcal{F}}^C_{\boldsymbol{N}_{ef}}(\boldsymbol{\mathcal{U}}_f^-, \boldsymbol{\mathcal{U}}_f^+)\, \|\boldsymbol{C}_{ef}\|. \tag{4}$$

$\Omega_0^e$ denotes the control volume of cell $e$, $\Lambda_e^f$ represents the set of surfaces $f$ of cell $e$, $\boldsymbol{N}_{ef} := \boldsymbol{C}_{ef}/\|\boldsymbol{C}_{ef}\|$ and $\|\boldsymbol{C}_{ef}\|$ denote the material unit outward surface normal and the surface area at face $f$ of cell $e$, and $\boldsymbol{\mathcal{F}}^C_{\boldsymbol{N}_{ef}}(\boldsymbol{\mathcal{U}}_f^-, \boldsymbol{\mathcal{U}}_f^+)$ represents the numerical flux computed using the left and right states of variable $\boldsymbol{\mathcal{U}}$ at face $f$, namely $\boldsymbol{\mathcal{U}}_f^-$ and $\boldsymbol{\mathcal{U}}_f^+$. Specifically, acoustic Riemann solver [1, 2] and appropriate monotonicity-preserving linear reconstruction procedure [1] are used for flux evaluation.

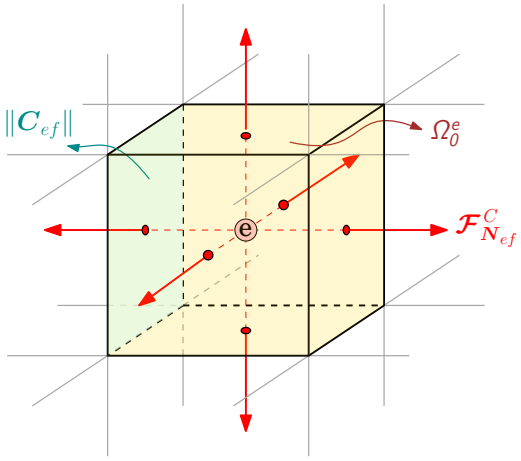


Figure 1: Cell centred Finite Volume Method

From the time discretisation viewpoint, an explicit one-step two-stage Total Variation Diminishing Runge-Kutta time integrator [1] has been employed in order to update the semi-discrete system (4).

# 4 Numerical results

## 4.1 *Parallel performance*

A standard benchmark problem of a twisting column is considered (see References [2, 3, 8, 10, 12] for details). The unit squared cross section column is twisted with a sinusoidal angular velocity field given by $\boldsymbol{\omega}_0 = \Omega[0, \sin(\pi Y/2H), 0]^T$ rad/s, where $\Omega = 105$ rad/s is the initial angular velocity and $H = 6$ m is the height of column.

The main aim of this example is to assess the parallel performance of the proposed tool-kit. Speedup analysis measures the improvement in execution time of a task and is defined as the ratio of serial execution time ($T_s$) to parallel execution time ($T_p$). The parallel speedup against the serial run is computed for this problem and is shown in Fig. 2a on a logarithmic scale depicting excellent scalability. It can be seen that for a mesh comprising of relatively coarse 48000 elements, the speedup increases until 256 cores are employed. When 512 processors are utilised, a significant dip in speedup is observed, stipulating that a bottleneck is achieved. However, as expected a significantly higher speedup is noticed when the problem size is increased to 6 million elements. It can be easily observed in Fig. 2a that for 512 cores an overall speedup of over 200 is obtained. Another terminology often used in parallel computing is the efficiency which monitors the speedup per processor. This becomes necessary when efficient utilisation of computational resources is of paramount importance. Fig. 2b shows the parallel efficiency of the proposed solid dynamics tool-kit.

## 4.2 *Biomedical stent*

In this section, a biomedical stent [1] (see Fig. 3a) is presented. This stent-like structure has an initial outer diameter of $D_O = 10$ mm, a thickness of $T = 0.1$ mm and a total length of $L = 20$ mm. For clarity, the dimensions of one of the repeated patterns on a planar surface are shown in Fig. 3b. A constant traction $\boldsymbol{t}_b = [0, 0, t]^T$ kPa where $t = -100$ kPa is applied at the top and bottom of the structure along the $X$-$Z$ plane. Due to the presence of three symmetry planes, one eighth of the problem is simulated with appropriate

[1] The CAD is freely available at www.grabcad.com/library/biomedical-stent-1.

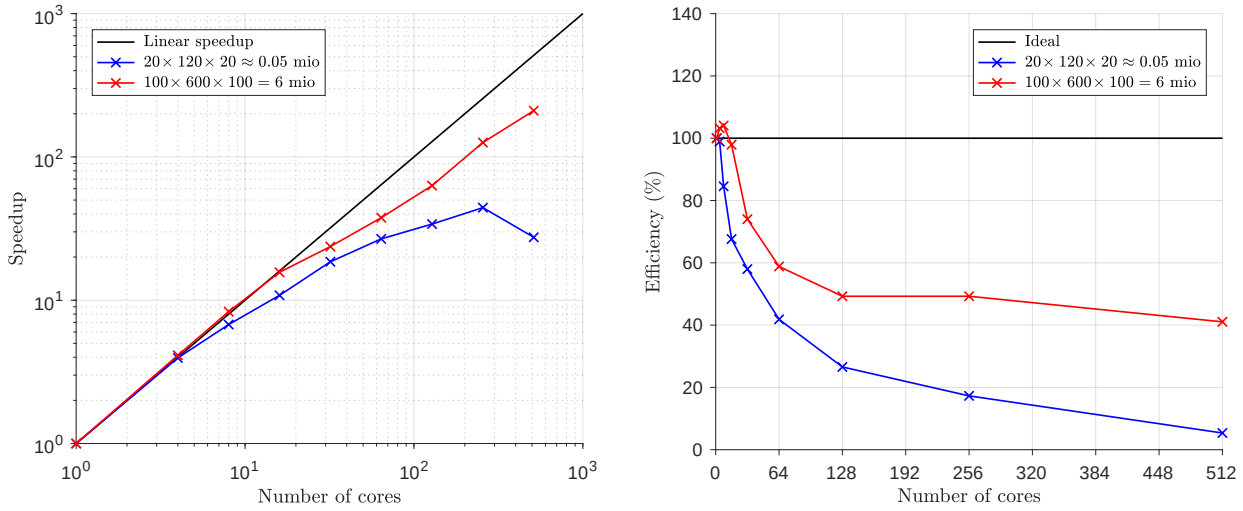


(a) Speedup

(b) Efficiency

Figure 2: Twisting column: (a) Parallel speedup; and (b) parallel efficiency tests for various meshes.

boundary conditions. The structure is modelled with a neo-Hookean material defined with density $\rho_0 = 1100$ kg/m$^3$, Young's Modulus $E = 17$ MPa and Poisson's ratio $\nu = 0.45$.

Fig. 4 shows the overall deformation of the structure at time $t = 500\,\mu$s, with zoomed views in critical areas of sharp spatial gradients. Very smooth pressure field is observed around sharp corners of the structure. To further examine the robustness of the algorithm, the problem is simulated with a larger value of Poisson's ratio $\nu = 0.499$. As can be observed in the first row of Fig. 5, the pressure field is plotted constant per cell without resorting to any sort of visual nodal interpolation. Alternatively, a nodal averaging process could also be used to display the results, refer to the second row of Fig. 5.

### 4.3 *Imploding bottle*

In order to assess robustness of the proposed solver, a challenging problem involving the implosion of a bottle [2] with initial height $H = 0.192$ m and initial outer diameter $D_0 = 0.102$ m is examined (see Fig. 6a). The bottle of thickness $T = 1$ mm is subjected to a uniform internal pressure of $p = 2000$ on the side walls thereby creating a suction effect (see Fig. 6b). Due to the presence of two symmetry planes, only a quarter of the domain is simulated. A neo-Hookean constitutive model is utilised where the material properties are density $\rho_0 = 1100$ kg/m$^3$, Young's Modulus $E = 17$ MPa and Poisson's ratio $\nu = 0.3$.

In Fig. 8, successively refined meshes comprising of 106848, 251896 and 435960 hexahedral elements are used and compared. A quarter of the domain is purposely hidden in Fig. 8b to highlight the smooth pressure representation in the interior of the bottle. As expected, when the mesh density is increased, convergence for deformed shape and pressure distribution can be observed. A significant change in the deformation of bottle is observed as the mesh density is increased from 106848 to 251896 elements. Further refinement ensures that the deformation pattern and the pressure distribution remains practically identical thus guaranteeing mesh independence. For visualisation purposes, time evolution of the implosion process using the refined mesh of 435960 elements is illustrated in Fig. 7. Very smooth pressure distribution is observed.

[2] The CAD is freely available at www.grabcad.com/library/bottle-456.

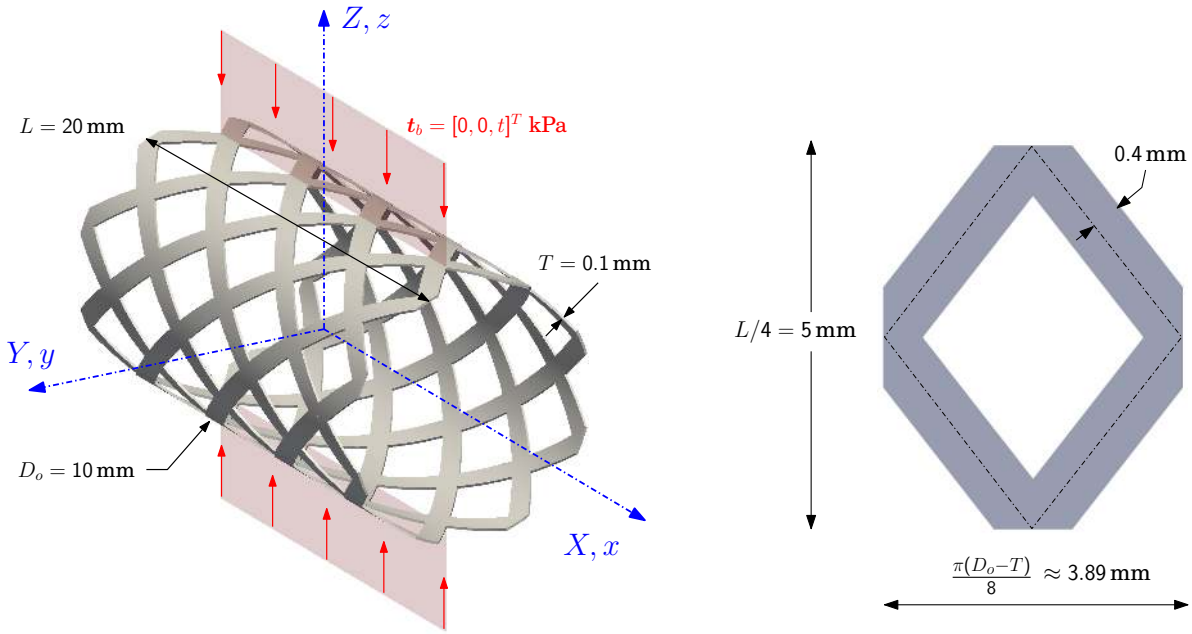


(a) Initial configuration

(b) Planar $1/32^{\text{th}}$ geometry

Figure 3: Biomedical stent: Problem setup.

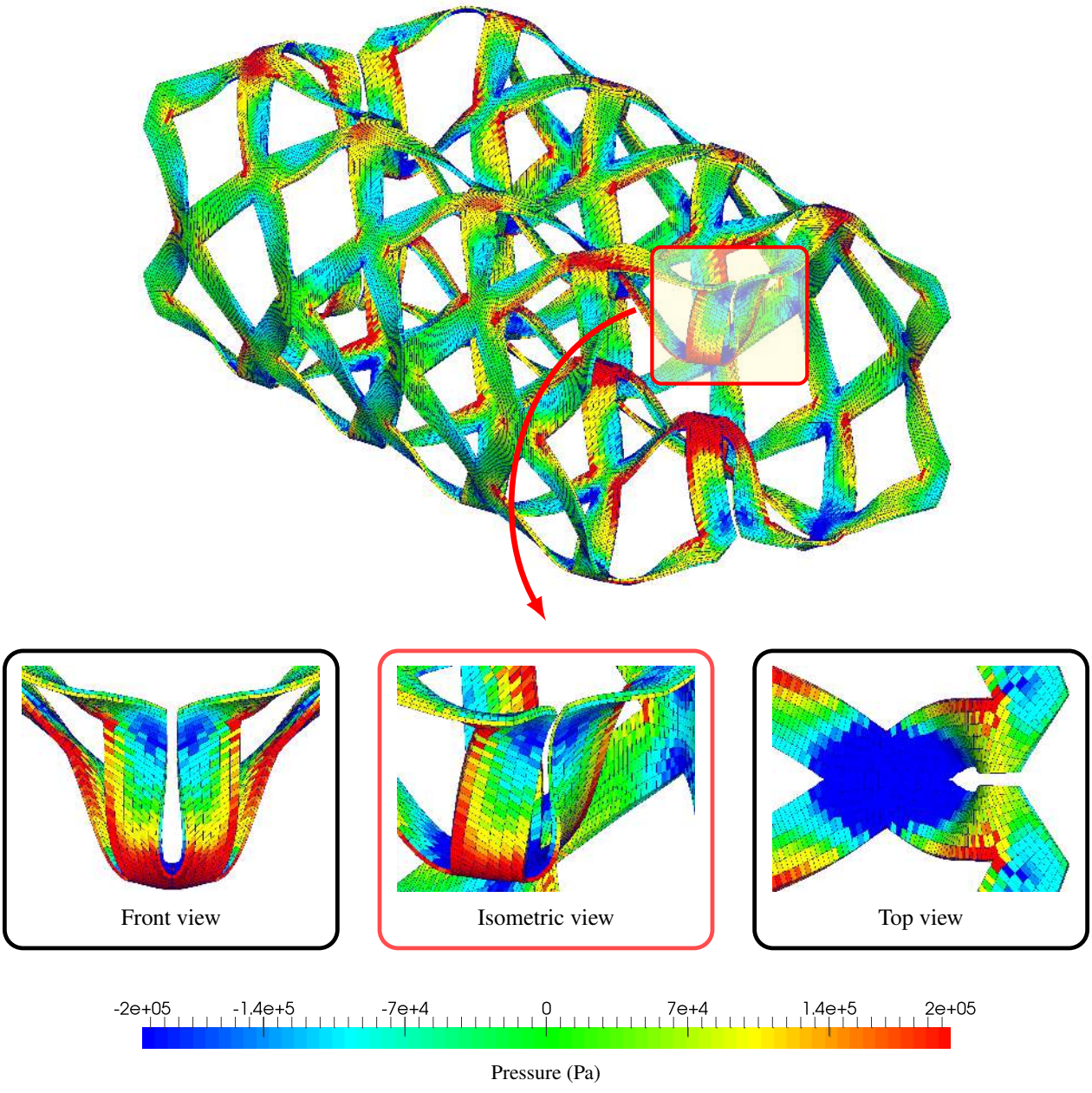


Figure 4: Biomedical stent: Snapshot of deformed shape highlighting the pressure distribution in key region at time $t = 500\,\mu$s. Results obtained with a discretisation of 6912 hexahedral elements using traction loading $\boldsymbol{t}_b = [0, 0, -100]^T$ kPa. A neo-Hookean material is used with $\rho_0 = 1100$ kg/m$^3$, $E = 17$ MPa, $\nu = 0.45$ and $\alpha_{\text{CFL}} = 0.3$.

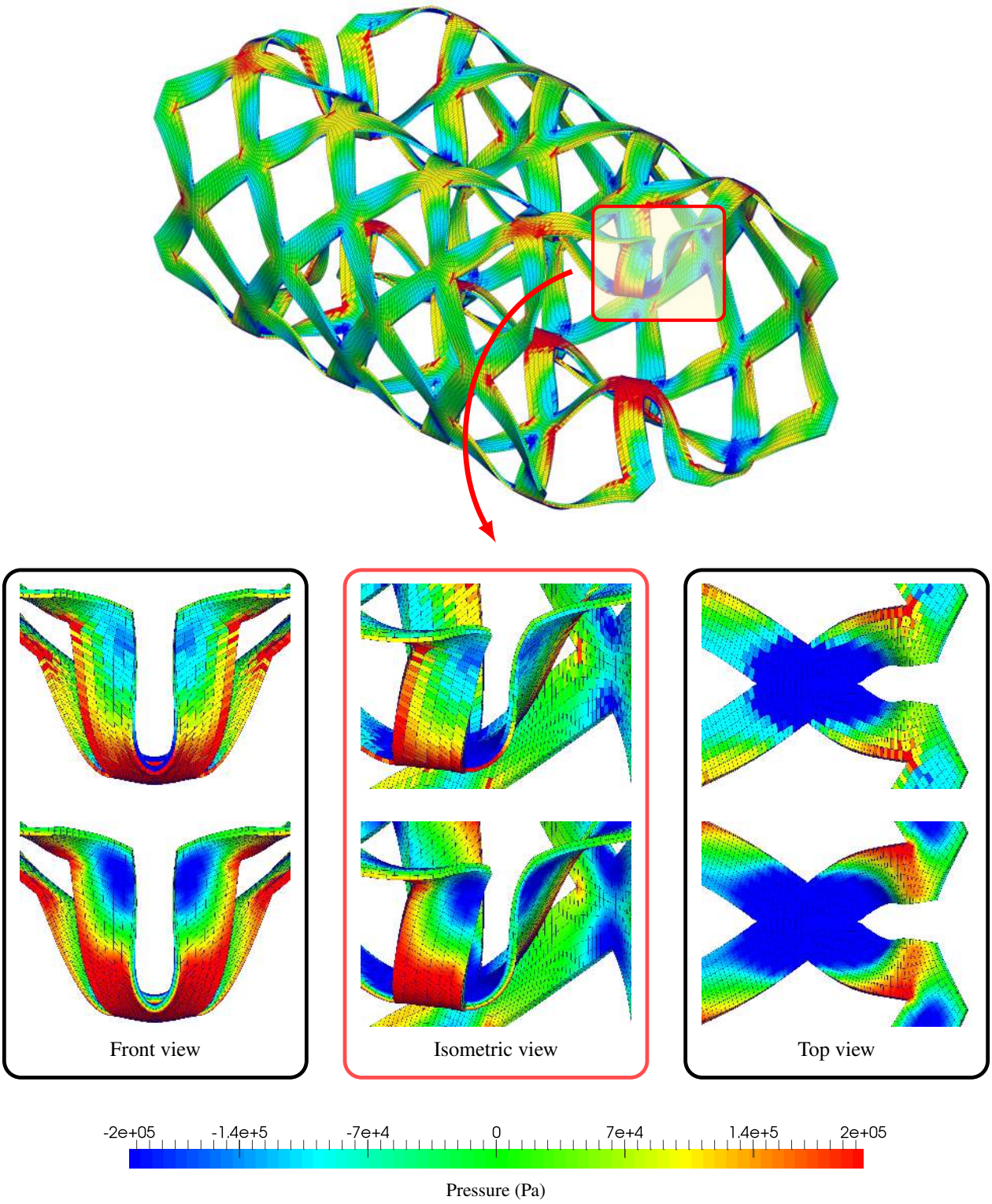


Figure 5: Biomedical stent: Snapshot of deformed shape highlighting the pressure distribution in key region at time $t = 500\,\mu$s. The first row shows the cell center pressure whereas the second row displays the interpolated/extrapolated pressure at the nodes. Results obtained with a discretisation of 6912 hexahedral elements using traction loading $\boldsymbol{t}_b = [0, 0, -100]^T$ kPa. A neo-Hookean material is used with $\rho_0 = 1100$ kg/m$^3$, $E = 17$ MPa, $\nu = 0.499$ and $\alpha_{\text{CFL}} = 0.3$.

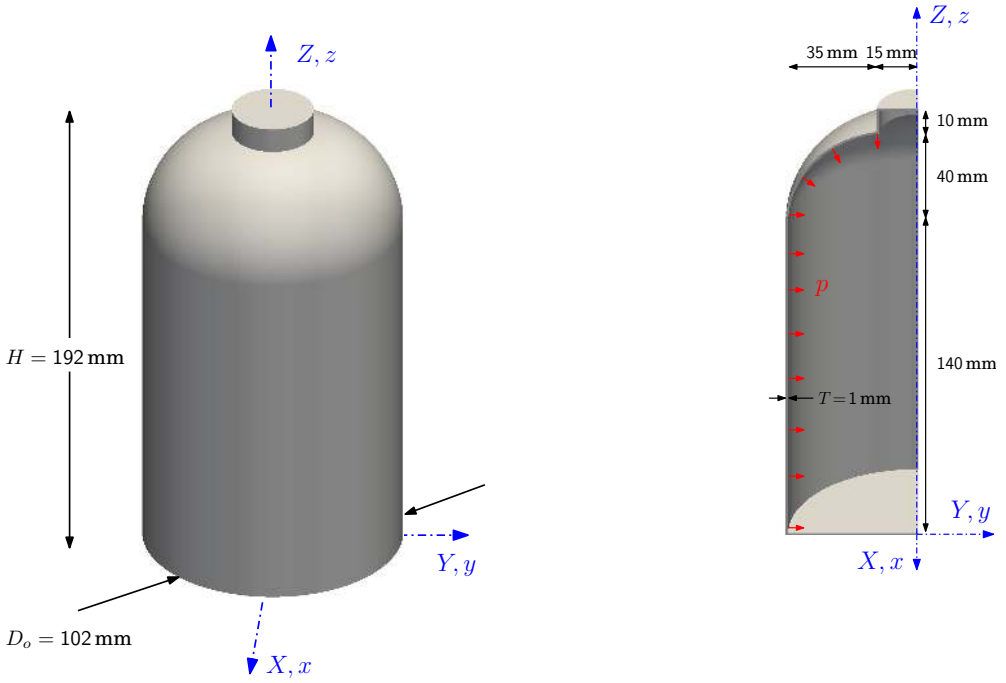


(a) Initial configuration

(b) Cross-section profile

Figure 6: Bottle: Problem setup.

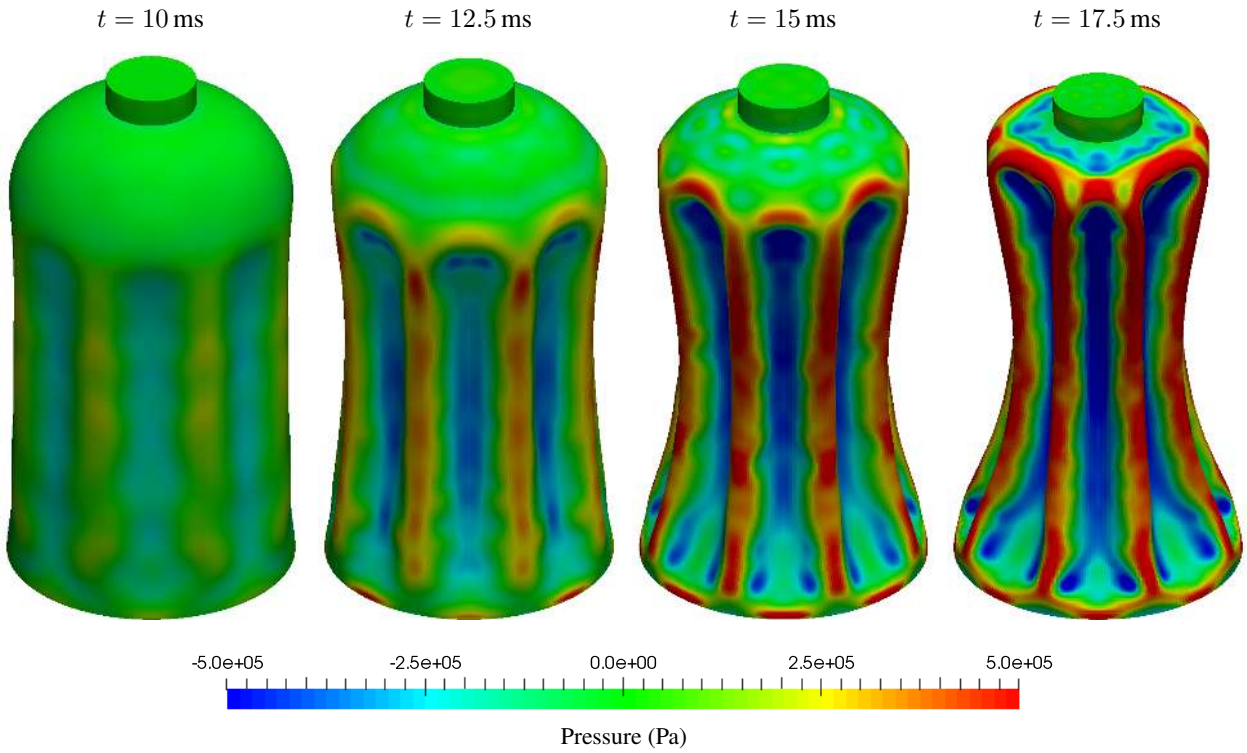


Figure 7: Imploding bottle: Time evolution of the deformation along with the pressure distribution. Results obtained with a suction pressure $p = 2000$ pa on the interior side walls using 435960 hexahedral elements in quarter domain. A neo-Hookean constitutive model is used with $\rho_0 = 1100$ kg/m$^3$, $E = 17$ MPa, $\nu = 0.3$ and $\alpha_{\text{CFL}} = 0.3$.

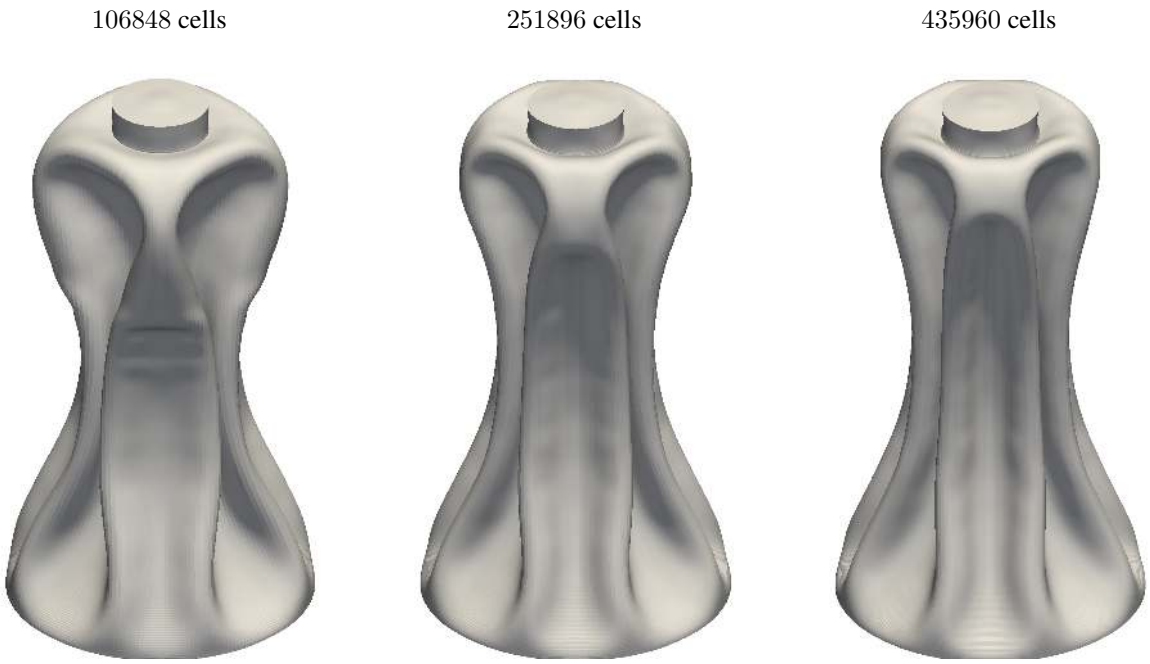


(a) Deformation

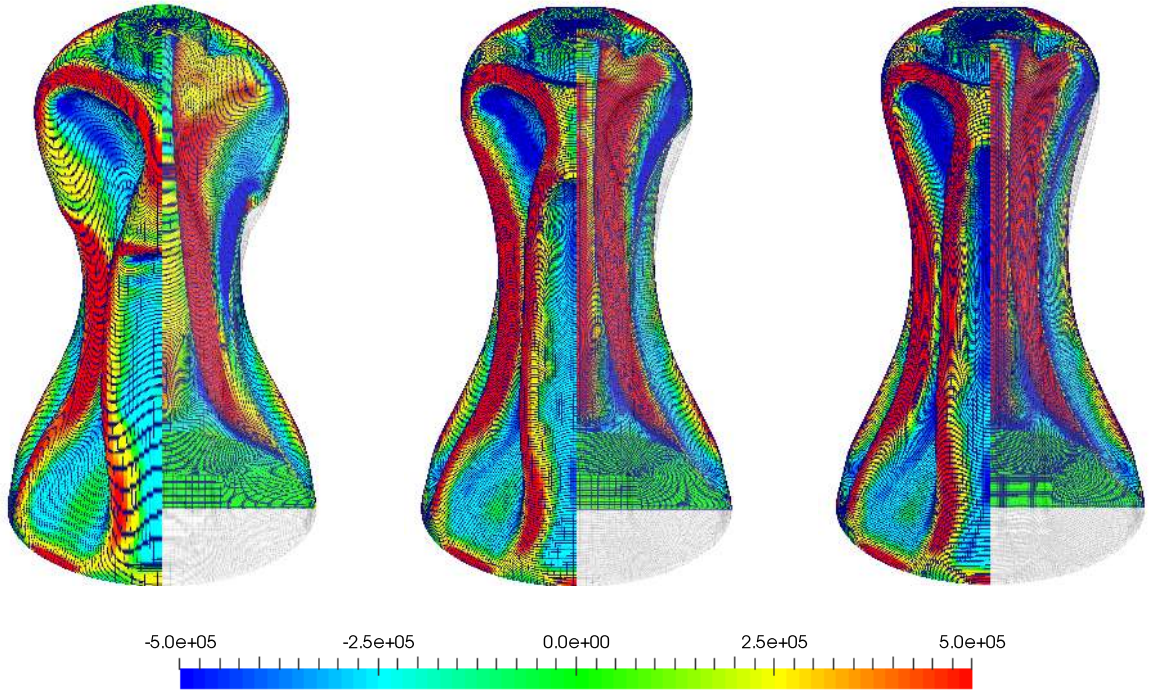


(b) Pressure (Pa)

Figure 8: Imploding bottle: Mesh refinement showing (a) deformed shape; and (b) pressure distribution at time $t = 19$ ms. Results obtained with a suction pressure $p = 2000$ pa on the interior side walls using meshes comprising of 106848, 251896 and 435960 hexahedral elements in quarter domain. A neo-Hookean constitutive model is used with $\rho_0 = 1100$ kg/m$^3$, $E = 17$ MPa, $\nu = 0.3$ and $\alpha_{\text{CFL}} = 0.3$.

### 4.4 *Crushing cylinder*

In this last example, a thin cylindrical shell, of outer diameter $D_0 = 200\,\text{mm}$ and height $H = 113.9\,\text{mm}$ (see Fig. 9a), is considered. The ratio of shell outer diameter to its thickness $T = 0.247\,\text{mm}$ is approximately 800 ($D_o/T \approx 800$) which makes this problem extremely challenging. In this case, the shell is simulated by applying a time varying velocity profile (see Fig. 9b) to the top surface described as

$$\boldsymbol{v}_b = \frac{\boldsymbol{d}_b}{t_{\text{max}}^3}\left[10\,t^2 - \frac{60\,t^3}{t_{\text{max}}} + \frac{30\,t^4}{t_{\text{max}}^2}\right]\ \text{m/s}, \tag{5}$$

where $t_{\text{max}} = 0.005\,\text{s}$ is the simulation end time and $\boldsymbol{d}_b = [0, d_{\text{max}}, 0]^T\,\text{m}$ is the total boundary displacement vector at $t = t_{\text{max}}$ where $d_{\text{max}} = -0.0045\,\text{m}$. A neo-Hookean constitutive model is used with density $\rho_0 = 1000\,\text{kg/m}^3$, Young's Modulus $E = 5.56\,\text{GPa}$ and Poisson's ratio $\nu = 0.3$.

A mesh refinement analysis is undertaken in Fig. 10, with the aim to show that the solution is mesh independent. As the mesh density is increased from 9000 cells to 160000 cells (see Fig. 10), a noticeable change in both the deformed shape and the pressure distribution at time $t = 5\,\text{ms}$ can be observed. However, similar deformation patterns and pressure field can be seen by further refining the mesh to 25000 elements. Remarkably, only two elements across the thickness have been used in all meshes for this problem. Moreover, in Fig. 11 a time evolution of the crushing process is depicted showing the various modes of deformation. Despite being a tough engineering problem to simulate, no pressure checker-boarding is observed.

## 5 Conclusions

This paper introduces a computationally efficient and industry-driven framework for the numerical simulation of large strain solid dynamics problems. Following the works of [1, 2, 3], a mixed formulation written in the form of a system of first order hyperbolic equations is employed where the linear momentum $\boldsymbol{p}$ and the deformation gradient $\boldsymbol{F}$ are the primary conservation variables of this mixed-based approach. This formulation has an eye on bridging the gap between Computational Fluid Dynamics and large strain solid dynamics. An acoustic Riemann solver has been employed for the evaluation of numerical fluxes. The proposed solid dynamics tool-kit has been implemented from scratch within the modern Computational Fluid Dynamics code OpenFOAM. Moreover, it is ensured that this tool-kit can be utilised on a parallel architecture and is compatible with the latest OpenFOAM Foundation release (OpenFOAM v5.0). Finally, a comprehensive list of challenging numerical examples are presented, highlighting the excellent performance of the proposed solver in large strain solid dynamics without any numerical instabilities.

## 6 Acknowledgements

The first author acknowledges the financial support provided by "The Erasmus Mundus Joint Doctorate SEED" programme and the European Regional Development Fund (ERDF) funded project "ASTUTE 2020 Operation". The second and third authors would like to acknowledge the financial support received through the Sér Cymru National Research Network for Advanced Engineering and Materials, United Kingdom.

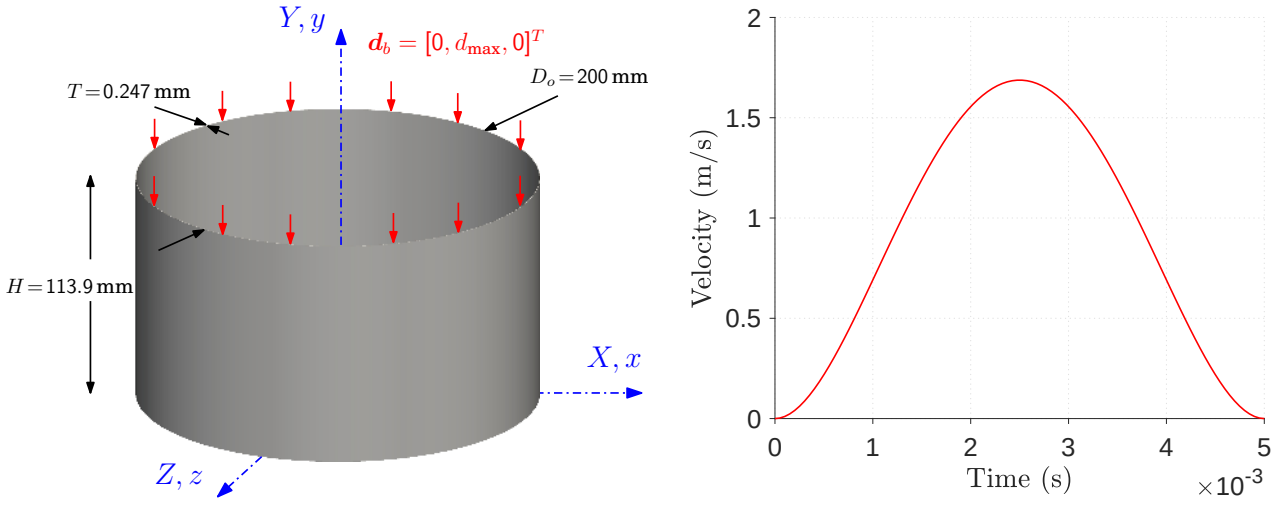


(a) Initial configuration

(b) Velocity profile

Figure 9: Crushing cylinder: Problem setup.

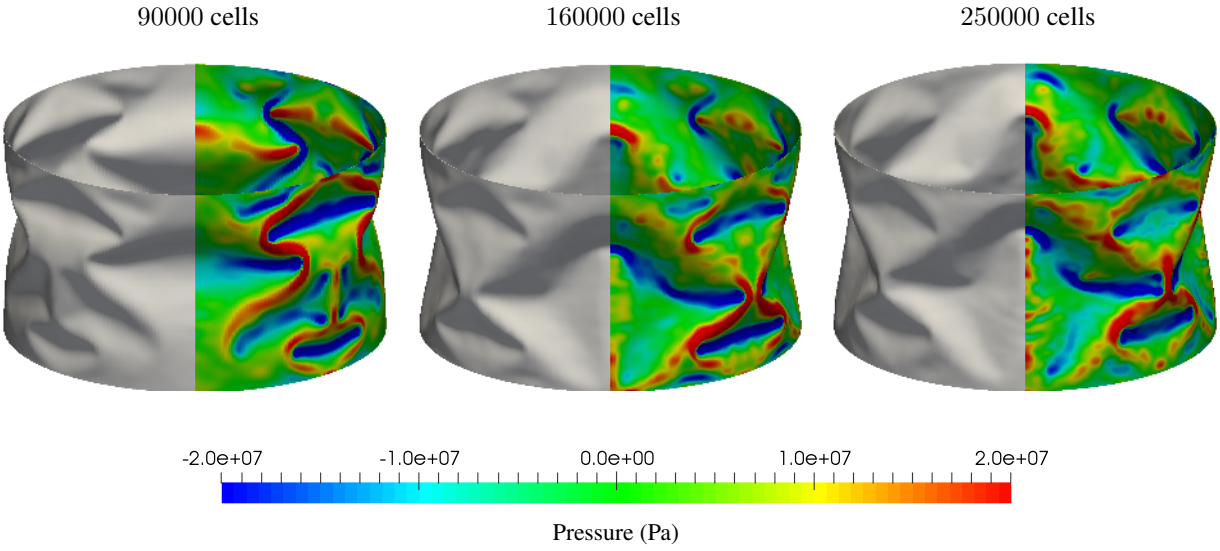


Figure 10: Crushing cylinder: Mesh refinement showing deformation (left half) and pressure distribution (right half) at time $t = 5$ ms. Results obtained by applying a time varying velocity profile on the top surface using 90000, 160000 and 250000 structured hexahedral elements in the quarter domain. A neo-Hookean constitutive model is used with $\rho_0 = 1000$ kg/m$^3$, $E = 5.56$ GPa, $\nu = 0.3$ and $\alpha_{\text{CFL}} = 0.3$.

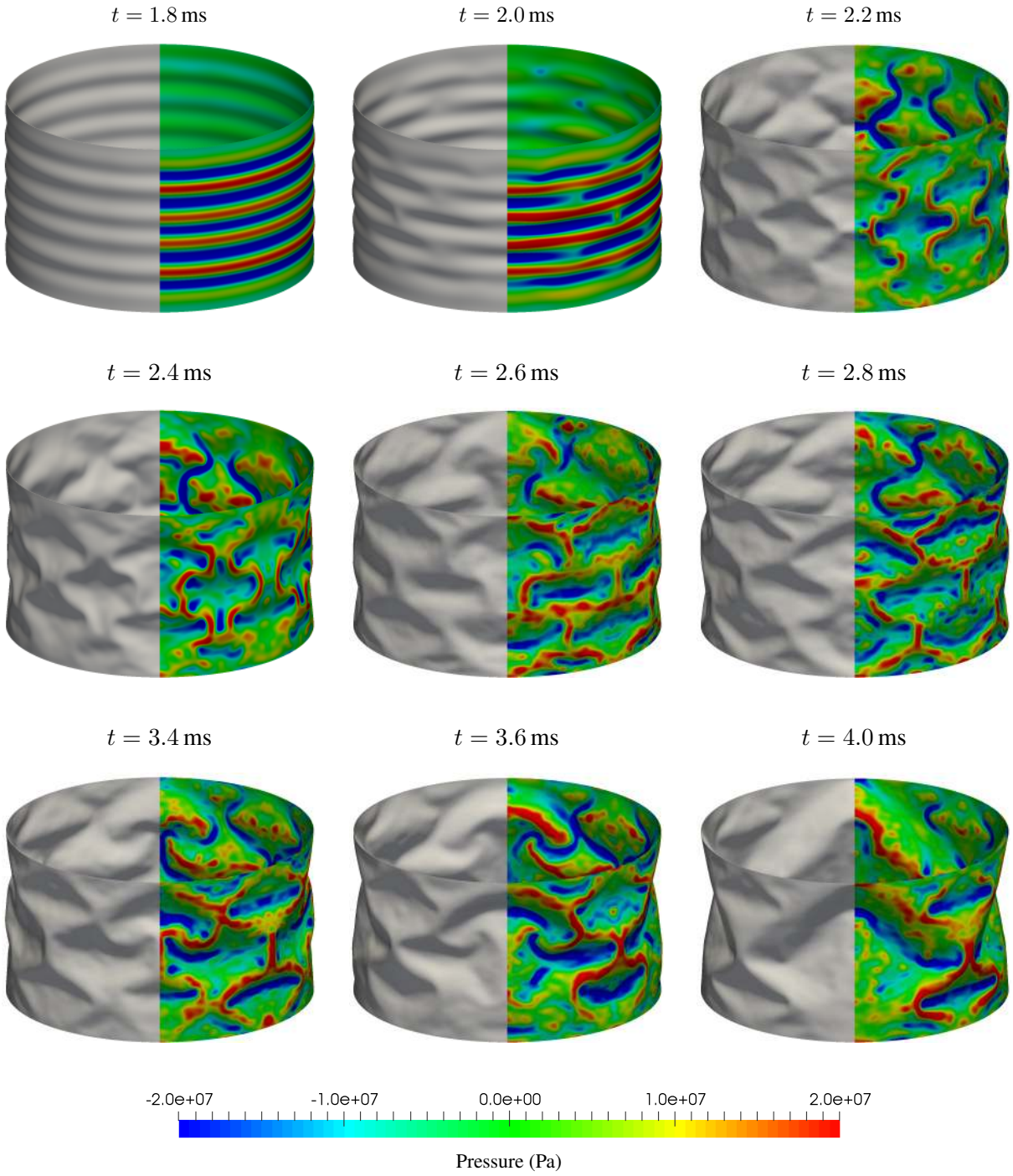


Figure 11: Crushing cylinder: Time evolution showing deformation (left half) and pressure distribution (right half). Results obtained by applying a time varying velocity profile on the top surface using 250000 structured hexahedral elements in the quarter domain. A neo-Hookean constitutive model is used with $\rho_0 = 1000$ kg/m$^3$, $E = 5.56$ GPa, $\nu = 0.3$ and $\alpha_{\text{CFL}} = 0.3$.

## References


[1] C. H. Lee, A. J. Gil, J. Bonet, Development of a cell centred upwind finite volume algorithm for a new conservation law formulation in structural dynamics, Computers and Structures 118 (2013) 13–38.

[2] J. Haider, C. H. Lee, A. J. Gil, J. Bonet, A first order hyperbolic framework for large strain computational solid dynamics: An upwind cell centred Total Lagrangian scheme, International Journal for Numerical Methods in Engineering 109 (2017) 407–456.

[3] J. Haider, C. H. Lee, A. J. Gil, A. Huerta, J. Bonet, An upwind cell centred Total Lagrangian finite volume algorithm for nearly incompressible explicit fast solid dynamic applications, Computer Methods in Applied Mechanics and Engineering (2018). https://doi.org/10.1016/j.cma.2018.06.010.

[4] H. Jasak, H. G. Weller, Application of the finite volume method and unstructured meshes to linear elasticity, International Journal for Numerical Methods in Engineering 48 (2000) 267–287.

[5] P. Cardiff, A. Karač, A. Ivanković, Development of a finite volume contact solver based on the penalty method, Computational Materials Science 64 (2012) 283–284.

[6] P. Cardiff, A. Karač, A. Ivanković, A large strain finite volume method for orthotropic bodies with general material orientations, Computer Methods in Applied Mechanics and Engineering 268 (2014) 318–335.

[7] C. H. Lee, A. J. Gil, J. Bonet, Development of a stabilised Petrov–Galerkin formulation for conservation laws in Lagrangian fast solid dynamics, Computer Methods in Applied Mechanics and Engineering 268 (2014) 40–64.

[8] A. J. Gil, C. H. Lee, J. Bonet, M. Aguirre, A stabilised Petrov–Galerkin formulation for linear tetrahedral elements in compressible, nearly incompressible and truly incompressible fast dynamics, Computer Methods in Applied Mechanics and Engineering 276 (2014) 659–690.

[9] A. J. Gil, C. H. Lee, J. Bonet, R. Ortigosa, A first order hyperbolic framework for large strain computational solid dynamics. Part II: Total Lagrangian compressible, nearly incompressible and truly incompressible elasticity, Computer Methods in Applied Mechanics and Engineering 300 (2016) 146–181.

[10] J. Bonet, A. J. Gil, C. H. Lee, M. Aguirre, R. Ortigosa, A first order hyperbolic framework for large strain computational solid dynamics. Part I: Total Lagrangian isothermal elasticity, Computer Methods in Applied Mechanics and Engineering 283 (2015) 689–732.

[11] M. Aguirre, A. J. Gil, J. Bonet, A. A. Carreño, A vertex centred finite volume Jameson–Schmidt–Turkel (JST) algorithm for a mixed conservation formulation in solid dynamics, Journal of Computational Physics 259 (2014) 672–699.

[12] M. Aguirre, A. J. Gil, J. Bonet, C. H. Lee, An upwind vertex centred Finite Volume solver for Lagrangian solid dynamics, Journal of Computational Physics 300 (2015) 387–422.